UNITED NATIONS UNIVERSITY
UNU-GTP
Geothermal Training Programme

Orkustofnun, Grensasvegur 9,
IS-108 Reykjavik, Iceland

Reports 2015
Number 22

EVALUATION OF STRUCTURAL PERMEABILITY IN MAHANAGDONG GEOTHERMAL FIELD, PHILIPPINES USING SOIL GASES (^{220}Rn, ^{222}Rn, CO_2 FLUX)

Jigo W. Mismanos
Geosciences and Reservoir Engineering Group
Energy Development Corporation – EDC
38/F One Corporate Centre, Julia Vargas corner Meralco Avenue
OrtigasCenter, Pasig City 1605
PHILIPPINES
mismanos.jw@energy.com.ph

ABSTRACT

The use of soil gases as a geologic tracer has long been elaborately demonstrated in several volcanic, seismic, and geothermal studies. Carbon dioxide (CO_2) is an abundant geothermal gas while radon (^{222}Rn) and thoron (^{220}Rn) are radioactive gases with a half-life of 3.8 days and 55 seconds, respectively. In theory, anomalous radon, thoron, and CO_2 gas emissions can be indicative of rapid vertical transport through permeable structures that serve as pathways of degassing. These gas anomalies can indicate structures, reservoir changes and processes. The application of soil gas mapping to permeability exploration was tested in production, reinjection, and undeveloped areas in Mahanagdong Geothermal Field, Leyte, Philippines. Most soil gas anomalies were observed at structural intersections and segments that were reported by drilling to exhibit good permeability. The concurrence of soil gas anomalies at fault traces indicated the presence of highly permeable structures that can be targeted for drilling exploration or make-up/replacement wells.

1. INTRODUCTION

The Leyte Geothermal Field, the world's largest liquid-dominated geothermal system, is situated in Leyte Island in central Philippines (Figure 1). The field consists of two distinct convection systems: the Mahiao-Sambaloran-Malitbog-Tongonan system and the Mahanagdong system, separated by a cold (<200°C) impermeable block (Seastres Jr. et al., 1996). The exploration and development of the geothermal field began in the late 1970s and currently has an installed capacity of more than 700 MWe, supplying electricity to the nearby islands and Luzon.

The geothermal system is related to Quaternary volcanism spawned by the subduction of the Philippine Sea Plate under the Philippine Mobile Belt. The geothermal reservoir is composed of Miocene-Pleistocene volcano-sedimentary units intruded by microdioritic dikes (Ward, 1979). The northwest-southeast oriented left-lateral strike-slip Philippine Fault, which transects the island, forms splays across the geothermal system. Parallel splays of the Philippine Fault within the Leyte Geothermal Field are complimented by conjugate faults oriented northeast-southwest (Delfin and Tebar, 1986). This dense,

interconnected structural network is the main source of permeability in the geothermal reservoir (Caranto and Jara, 2015). Conventional geologic mapping can be surmised to be successful in mapping these permeable fluid-bearing structures, as evidenced by the calculated encounters with highly productive intercepts and zones, but now other methods that can corroborate permeability are also being considered, such as geophysical imaging and soil gas mapping.

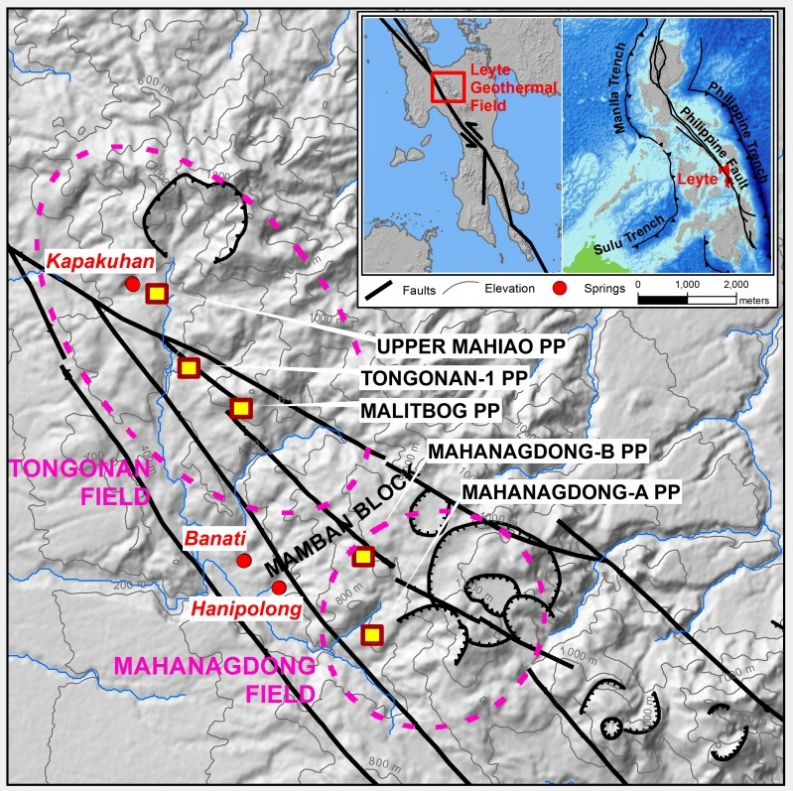

FIGURE 1: Location map of Mahanagdong Geothermal Field, Leyte island, Philippines

Soil gases have long been studied for various geoscientific and environmental applications. Surveys employing soil gases are anchored on the principle that gases from a deep source (e.g. a degassing magma body, decay of radioactive minerals) are also released through permeable pathways, or diffuse soil emanations aside from concentrated point sources such as volcanic vents and fumaroles (Allard et al., 1991). Previous works demonstrated interest in the fluctuations of soil gas concentrations as a function of volcanic/seismic activity (Brusca et al., 2004; Heiligmann et al., 1997) or meteorological variability (Hinkle, 1991; Rinaldi et al., 2012). In geothermal applications, mapping soil gas anomalies has been used to delineate a geothermal system (Cox, 1980; Lewicki and Oldenburg, 2004; Voltattorni et al., 2010) and map permeable structures (Jolie et al., 2015; Padrón et al., 2003; Rodríguez et al., 2008), or aid in field monitoring in the advanced phases (Fridriksson et al., 2006; Bergfeld et al., 2001). Usually, one or a combination of soil gases are considered in a study, but perhaps the most commonly used gases are carbon dioxide and radon. Beside their innate physicochemical properties as geologic tracers, detection of these gases in the field can be achieved with adequate accuracy.

Carbon dioxide (CO_2) is the second most abundant gas in volcanic emissions, accounting for 10% to 40% of total molar gas content after water, which normally comprises more than 60% of the vapour phase (Delmelle and Stix, 1999). In geothermal systems, carbon dioxide generally constitutes 80% w/w of all gases excluding steam (Mahon et al., 1980). Elevated carbon dioxide fluxes in soil have been measured above geothermal resources, typically at hot grounds and faults/structures (Chiodini et al., 1998; Klusman et al., 2000) but anomalous CO_2 fluxes have also been encountered above main upflow zones (Werner and Cardellini, 2006). In developed geothermal fields, elevated soil CO_2 fluxes have been associated with the onset of or continuous fluid extraction, resulting in the expansion of the steam zone and increased heat flow to the surface (Bergfeld et al., 2001; Hinkle, 1991; Óladóttir and Fridriksson, 2015).

Radon is a radioactive noble gas formed from the decay of uranium. ^{222}Rn (radon), the most abundant isotope, is a part of the ^{238}U decay series and has a half-life of only 3.8 days. Another isotope of radon, ^{220}Rn, occurs as an intermediate step in the ^{232}Th (thorium) decay series, thereby acquiring the name thoron. It has a much shorter half-life of only 55.6 seconds. Parent nuclides of ^{222}Rn and ^{220}Rn (^{238}U to ^{224}Ra and ^{232}Th to ^{226}Ra, respectively) occur naturally in trace concentrations in most rock types (Parker,

1967). Thus, the emanation of radon gas from rock matrix to reservoir pore volume ensures a steady and constant influx of radon to the geothermal fluids (Semprini and Kruger, 1983).

In sub-terrestrial settings, radon can migrate by diffusion and/or convection (Tanner, 1980). Because of the short half-life of radon, diffusion can only facilitate short distances of transportation before significant decay takes place (McCarthy and Reimer, 1986). Rapid extraction of large amounts of radon from deeper origins is generally made possible by convection (Witcher, 1991; Cox, 1980). Since thoron has a much shorter half-life, its diffusive length is extremely limited to orders of centimetres (Fleischer and Mogro-Campero, 1978). Thus, it is useful only in areas where convective flow is considerable. Permeable vertical conduits such as faults and fractures provide pathways of rapid bulk transport from depth to surface, where they can occur at levels higher than background (Voltattorni and Lombardi, 2010). In some studies, the different half-lives of ^{222}Rn and ^{220}Rn are used to estimate the depth of origin of gases, *i.e.*, a relatively deep source for ^{222}Rn, and shallow source for ^{220}Rn (Giammanco et al., 2009; Yang et al., 2005). For example, low radon/thoron ratios in soil gases over a fault trace have been inferred as indicative of shallower gas source (Yang et al., 2005).

In 2013, a soil radon survey campaign was conducted in Mahanagdong to investigate the correlation of soil radon anomalies with the permeability of structures that were intersected by wells (Mismanos and Vasquez, 2013). High radon anomalies were observed above surface traces of proven permeable structures. Based on this preliminary work, soil gas prospecting is seen as a potential method in identifying and locating permeable structures which can be targeted for drilling exploration or make-up and replacement wells in new or producing geothermal fields in the Philippines, or in Mahanagdong at least.

This study aims to investigate the relationship between radon and other soil gases and subsurface permeability in Mahanagdong geothermal field, specifically by examining the correlation of soil radon, thoron, and CO_2 flux anomalies with permeability reported from drilling of geothermal wells, in pursuance of the positive results of the initial radon survey. Moreover, this study seeks to assess the potential of soil gas exploration in delineating permeable structures or structural segments in undeveloped areas within a geothermal field, *i.e.*, sectors with no geothermal wells drilled yet.

2. METHODS

2.1 Study area

The soil gas surveys were conducted in selected sites in Mahanagdong Geothermal Field (Figure 2), using the same stations occupied by an initial radon survey campaign executed from February in May 2013 (Mismanos and Vasquez, 2013). The measurement stations are grid-spaced roughly 150 m from each other. The grid areas, having a combined area of 5.9 km^2, are (1) Area A, a production sector located inside an old flank collapse feature, where production wells have been drilled; (2) Area B, a reinjection sector where reinjection wells have been drilled; and (3) Area C, an unexploited area immediately southeast of Area B, which will be investigated for permeability. The survey campaign was carried out from February to March 2015 to coincide with the local dry season. In most cases, sampling stations are located in regions of thick vegetation and steep terrain.

As none of the stations manifested thermal anomalies, i.e. soil temperatures were never greater than ambient, measurements were also taken at three hot spring/fumarole areas located around Leyte geothermal field (Figure 1), namely Kapakuhan, Banat-i, and Hanipolong to characterize soil gas concentrations and fluxes in grounds with elevated temperature.

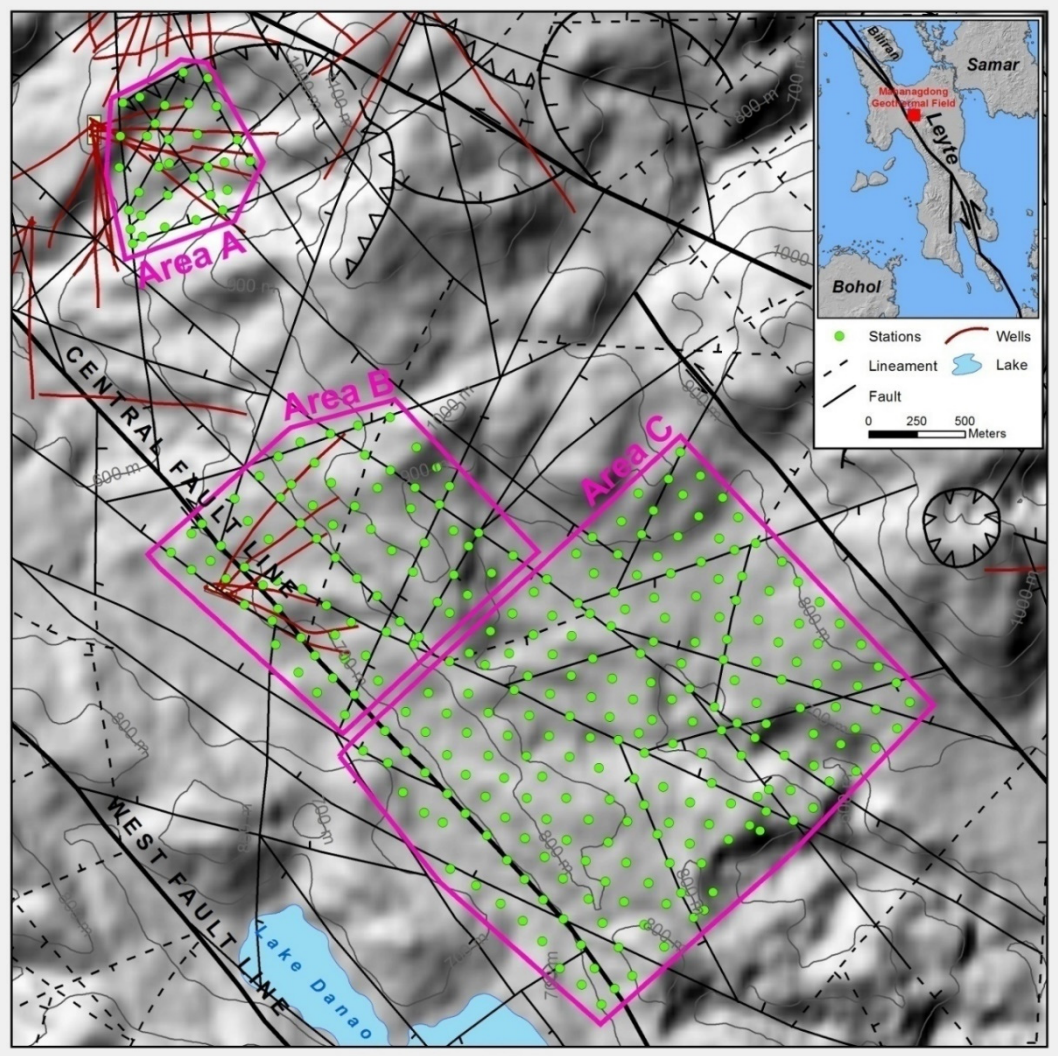

FIGURE 2: Soil gas grid surveys (enclosed in pink rectangles) at Mahanagdong geothermal field. From northwest to southeast: Area A, Area B, and Area C

2.2 Soil gas measurements

For each station, radon and thoron in soil gas and soil CO_2 flux were measured (Figure 3). In addition, GPS coordinates, soil air temperature and barometric pressure were recorded by the instruments, and observations on soil characteristics and prevailing weather were collected during the survey. Radon and thoron were measured using a radon detector with a pump and a steel probe (Figure 3). The instrument uses a solid-state alpha detector, which is a semiconductor material that converts alpha radiation directly to an electrical signal. The daughter isotopes of radon and thoron have different alpha energies and produce different strength signals in the detector, which is then identified through alpha emission spectroscopy. The steel probe is inserted vertically in the soil, down to 1 m depth and connected to the detector. Soil gas is pumped inside the detector chamber, where emissions are counted in five, 5 minute cycles. For radon, the first two cycles are disregarded to account for the response of its progeny, ^{218}Po (half life of 3.1 minutes). Radon and thoron concentrations are reported in the SI units becquerels per cubic meter (Bq/m^3), with 1 Bq/m^3 equivalent to one radioactive disintegration per second happening in one cubic meter of space. In contrast, the 2013 survey used a different instrument which operates using a diffusion chamber. It also relies on alpha spectroscopic detection, but instead of pumping the soil gas directly into the detection chamber, soil gases were allowed to diffuse through a silica membrane, thereby requiring a measurement duration longer than 60 minutes. Using the instrument with a diffusion

chamber to collect samples also introduces more soil perturbation because it requires a 4"-diameter-wide borehole, unlike the ¼" steel probe used in this survey which can easily be inserted in the ground.

FIGURE 3: Soil gas sampling for ^{222}Rn and ^{220}Rn using a radon detector with a soil gas probe (left) and CO_2 flux using an accumulation chamber (right) at Mahanagdong, Leyte

Soil CO_2 flux is measured using the accumulation chamber method (Figure 3). This technique is the most commonly used approach in soil respiration investigations as it is relatively inexpensive and adaptable to a wide range of field conditions and objectives (Rochette and Hutchinson, 2005). With this technique, flux is calculated from the rate of increase in CO_2 concentration observed within an inverted chamber placed on a soil surface. The instrument used is an accumulation chamber connected to an infrared gas analyzer for quantifying CO_2. One flux reading is taken in each station. A measurement takes 90 to 180 seconds until a flux curve with a good regression coefficient is attained. Soil CO_2 flux is initially measured as $mol \cdot m^{-2} \cdot d^{-1}$ and later converted to $g \cdot m^{-2} \cdot d^{-1}$ by multiplying the value with the molecular weight of CO_2 (44.01 g/mol).

2.3 Partitioning of anomalous soil gas populations

In order to identify possible threshold values of anomalous soil gas concentration and flux, the soil gas data was evaluated using probability plots following the graphical procedure of Sinclair (1974). The idea is to partition a polymodal data set into separate populations by identifying inflection points in a probability plot of soil gas data. In turn, these natural breaks in the data set can distinguish the anomaly of interest from the background signal. This method has been widely used in geochemical data sets, especially in soil gas studies where it is used to separate soil gases of hydrothermal or deep origin from soil gases of background processes or superficial origin.

2.4 Logistic regression

Whereas a good estimation of a soil gas anomaly threshold using partitioning is reliant on experiential visual perception of a probability graph (Sinclair, 1991), logistic regression depends on the correlation of soil gases with a parameter approximated by the anomaly. Logistic regression is suitable for predicting a dependent categorical/discrete variable from one or more independent predictors which can either be continuous or a mix of continuous and categorical variables. The general form of the logistic regression equation is:

$$P(y = 1|x_1, \dots x_i) = \frac{1}{1 + e^{-(\beta_0 + \beta_1 x_1 + \cdots \beta_i x_i)}} \quad (1)$$

where $P(y = 1|x_1, \dots x_i)$ = Probability of the desired outcome (*i.e.* dependent variable, y)
β_0 = Coefficient of the intercept
$\beta_1 \dots \beta_i$ = Coefficient of $x_1 \dots x_i$
$x_1 \dots x_i$ = Independent variable or predictor

The desired outcome is to predict “highly permeable” areas based on soil gas concentration values measured at the surface, with the assumption that vertical permeability is continuous. Using the derived model, a threshold value for soil gas concentration/flux can be calculated and used to assess the occurrence of structural permeability in unexploited areas. The database is populated with stations from the production and reinjection sectors that correspond to surface expressions of the intercept between drilled wells and faults. Based on evaluations of permeability from drilling, geology and completion tests, a value of "1" was set for stations positioned at intercepts with reported good permeability and "0" for stations located on intercepts with reported poor permeability. The input database for the model consists of the continuous variables (radon and thoron concentration, CO_2 flux), and discrete variable (permeability). Upon generation of a logistic regression model, a cut-off point shall be chosen based on balanced values of sensitivity and specificity and a robust overall percentage of correct classification (PCC). Sensitivity describes the proportion of positives that are correctly classified as positives, while specificity represents the proportion of negatives that are correctly classified as negatives. Meanwhile, the value of PCC takes into account the effect of both specificity and sensitivity. The cut-off point corresponding to the most optimized values of these three factors can be substituted to P in Equation 1 to get a threshold of the predictor. Based on the model, this “permeability threshold” is the borderline soil gas concentration differentiating between good permeability and poor permeability structures. In evaluating the best model, inspection of the AIC (Akaike Information Criterion) can aid the comparison between different models. The AIC is a measure of the probability of loss of information from the model, and deals with the compromise between the goodness of fit and the complexity of the model. A smaller AIC means that there’s a higher chance for the model to minimize loss of information. The R software was used to execute the logistic regression codes and build the regression model based on the generated parameters for each variable pair.

2.5 Soil gas maps

Interpolation of values between measurement nodes was done using sequential Gaussian simulation (sGs), which is a suitable tool to model soil diffused degassing (Frondini et al., 2004). The sGs method uses the dataset to generate a great number of equiprobable representations or realizations of the spatial distribution of soil gases. The sampled attribute is simulated at each unsampled location by random sampling of a Gaussian conditional cumulative distribution defined on the basis of the original data. The desired number of the equiprobable realizations is then generated and used in drawing a map representing the average of all simulations. The WinGslib software of Statios was used to process the interpolation of soil gas data. For each dataset, 100 realizations are calculated on a model grid with a 5 m grid spacing using the sGs code by Deutsch and Journel (1998), and the average value for each grid cell is presented on maps.

3. RESULTS

A total of 32, 75, and 207 soil gas measurements were collected from grid surveys at Area A, Area B, and Area C, respectively. A summary of the measurements, along with the radon measurements from 2013 is presented in Table 1.

For all three areas, radon concentrations measured in 2013 only amounted to less than half the value of the recent radon gas measurements. The difference is explained by the different instruments employed in these surveys. Analysis of the 2013 readings indicated that the counting duration could not have been optimized for the diffusion chamber instrument, despite the 90-minute duration of measurement, and/or that the soil perturbation from sampling induced compaction and reduction of soil permeability (Mismanos and Vasquez, 2013).

TABLE 1: Summary of soil gas measurements at Mahanagdong

	Year	Units	Area A	Area B	Area C
N			32	75	207
Radon (^{222}Rn)	2013	Bq/m^3	200–13300	80–21000	200–13400
Radon (^{222}Rn)	2015	Bq/m^3	136–31100	0–45300	0–45900
Thoron (^{220}Rn)	2015	Bq/m^3	0–16000	0–14900	0–23400
CO_2 Flux	2015	g·m^{-2}·d^{-1}	7.81–31.58	4.98–82.69	4.90–79.04

N = number of points

3.1 Soil gases in thermal areas

Soil gas measurements from Kapakuhan (KAP), Banat-i (BAN), and Hanipolong (HAN) thermal areas are shown in Table 2 below. Kapakuhan is an extensive thermal ground sprawled along a stream valley in Tongonan. Boiling mudpools, hot springs, and fumaroles are littered throughout this thermal area. Banat-i is situated at the northwestern edge of the Mahanagdong field and is characterized by 2 to 3 large vigorously boiling springs with disseminated hot grounds within less than a 100 m^2 area beside a stream. Hanipolong is located several hundred meters from Banat-i, and is characterized by large altered grounds and a mud pool. All measurements were taken at a certain distance from active manifestations where the substrate is not rocky or water-saturated.

TABLE 2: Soil gas concentrations and fluxes measured at thermal grounds

Name	Soil Temp *°C*	Radon *Bq/m^3*	Thoron *Bq/m^3*	^{222}Rn/^{220}Rn	CO_2 Flux *g·m^{-2}·d^{-1}*
KAP1	31.9	781	105	7.44	3.70
KAP2	40.2	2467	0.00	0.00	154.5
BAN1	31.3	205333	3033	67.69	23.42
BAN2	32.5	4417	4370	1.011	28.44
HAN1	31.6	19633	778	25.25	52.68
HAN1	32.2	16233	805	20.17	77.11

The measurements taken from the thermal areas show a wide range of values. In fact, the highest radon (205,333 Bq/m^3) and CO_2 flux (154.5 g·m^{-2}·d^{-1}) read in the whole survey came from Banat-i and Kapakuhan, respectively. While thermal areas are manifestations of permeability and obviously mark the presence of convective forces and abundant carrier gases, small and localized environments may exist that can exert control on the diffuse emanation of trace gases. For one, clay alterations can hold water and plug pores and fractures. In some instances, the high flux rate of carrier gas overwhelms the trace gases being detected by the instrument (Giammanco et al., 2009).

3.2 Soil gas anomaly threshold

Partitioning was done for each set of radon, thoron, and CO_2 flux data from the 2015 grid surveys. In general, the soil gas data are not normally distributed and highly skewed to the right. To assimilate a normal distribution, logarithmic transformation is applied to CO_2 flux and radon/thoron ratios, while cube root transformation is applied to radon and thoron data sets. These transformations were chosen to correct the positive skew of the data and take on a Gaussian-shaped distribution. At least two inflection points have been observed in most data sets (see Appendix I). A summary of the partitioned populations is also presented in Appendix II.

Populations representing the background are combined into a single group and presented in Table 3. Since the anomaly of interest is caused by unusual enrichment of gases or gas flux in soil, the populations

in the upper extremes are considered. These anomalous populations are thus defined from the inflections occurring at the uppermost quantiles of the data, with most of the anomalies generally occurring above the 80th percentile. From the table, different anomalies have been generated from each area due to the different characteristics of each data set.

TABLE 3: Partitioned populations from probability curves of Mahanagdong soil gas data sets

Gas	Characteristic	Area A			Area B			Area C		
		N_i	f_i (%)	Range	N_i	f_i (%)	Range	N_i	f_i (%)	Range
^{222}Rn	Anomaly	3	11.2%	11467–31100	9	12.8%	23300–45300	15	7.5%	25367–45900
	Background	29	88.8%	136–11467	66	87.2%	0–23300	192	92.5%	0–25367
^{220}Rn	Anomaly	3	11.2%	8510–11600	10	14.1%	9923–14900	21	10.4%	13000–23400
	Background	29	88.8%	0–8510	65	85.9%	0–9923	186	89.6%	0–13000
^{222}Rn/ ^{220}Rn	Anomaly	4	15.3%	2.32–3.74	7	10.6%	6.19–20.77	21	11.0%	4.17–61.03
	Background	26	84.7%	0.38–2.32	65	89.4%	0.27–6.19	175	89.0%	0.08–4.17
CO_2 Flux	Anomaly	3	11.2%	24.34–31.58	4	6.1%	32.1–82.69	7	3.7%	40.78–50.57
	Background	29	88.8%	7.81–24.34	71	93.9%	4.98–32.1	200	96.3%	4.90–40.78

N_i = size of population
f_i = proportion of population

3.3 Logistic regression and permeability threshold

The database for logistic regression was composed by projecting the well-fault intersection to its surface trace and matching it with the soil gas measurement at the corresponding station. Since faults are projected down to a range of dips, occasionally this approach gets crude when the well track is sub-parallel to the fault trace. Due to the close spacing of wells, there are instances where different well-fault intercepts share the same soil gas data. A summary of the data is presented in Table 4 below. The mean and the range (enclosed in parentheses) of good and poor permeability groups are shown in each field. Although there is a significant overlap between the two groups, the means can be considerably distant, e.g. radon, radon/thoron ratio.

TABLE 4: Summary of soil gas data used for logistic regression

Permeability	*N*	Radon (Bq/m^3)	Thoron (Bq/m^3)	Radon/Thoron	CO_2 Flux(g·m^{-2}·d^{-1})
Good (1)	20	13721 (1021-45300)	5717 (80-11667)	4.13 (1.03-15.13)	17.96 (4.98-38.24)
Poor (0)	34	5988 (591-25967)	5059 (0-16133)	1.19 (0-2.80)	16.19 (7.81-29.30)

Four models were considered in the logistic regression as a predictor of permeability. As shown in Table 5 below, these models are: a) Model A with permeability explained by radon concentration, b) Model B with permeability explained by thoron, c) Model C with permeability explained by the isotopic ratio of radon over thoron, and d) Model D with permeability explained by CO_2 flux. The parameters of the fitted models (β_0,β_1,AIC) generated using the R software, are also presented in Table 5 below.

TABLE 5: Generated parameters for the logistic regression models

Model	Definition	β_0	β_1	AIC	Cut-off	Sp	Se	PCC
A	P ~ ^{222}Rn	4.643×10^{-1}	6.031×10^{-5}	66.4	0.72	0.51	0.53	0.51
B	P ~ ^{220}Rn	4.032×10^{-1}	1.095×10^{-4}	66.6	0.70	0.64	0.40	0.57
C	P ~ ^{222}Rn/^{220}Rn	6.090×10^{-1}	1.775×10^{-1}	66.3	0.70	0.64	0.40	0.57
D	P ~ FCO_2	9.793×10^{-1}	-1.410×10^{-3}	67.8	0.70	1.00	0.00	0.72

AIC = Akaike Information Criterion; Sp = Specificity; Se = Sensitivity
PCC = Percent correct classification

For each model, the optimal cut-off and corresponding specificity, sensitivity, and PCC are also described. The values achieved by the model on these checks are below the rule-of-thumb value of 0.70. While Model A roughly balances sensitivity with specificity, Models B and C favour specificity. Model D, on the other hand, rates poorly on sensitivity. It is impossible to choose a good cut-off for Model D because it changes from strictly specific to strictly sensitive in just a small change in cut-off. For this reason, this model is not evaluated further in threshold estimation.

Substituting the parameters β_0, β_1, and selected cut-offs for each model to Equation 1 yields a threshold value of 7,962 Bq/m^3 for radon, 4,055 Bq/m^3 for thoron, and 1.34 for radon/thoron ratio (Table 6). The corresponding proportion of the population above the permeability threshold is also shown in Table6 above. Compared to the anomaly threshold obtained from partitioning, the permeability thresholds are much lower and in most cases encompass more than half of the population. As a result, this threshold estimation method is not narrowing down or pinpointing specific structures or structural segments for further investigation. For the succeeding sections, more focus shall be given to the anomaly threshold (from partitioning) in defining structural zones of interest.

TABLE 6: Calculated thresholds from the logistic regression models

Model	Definition	Threshold	% Population		
			Area A	Area B	Area C
A	P ~ ^{222}Rn	7962	25%	72%	53%
B	P ~ ^{220}Rn	4055	53%	64%	61%
C	P ~ ^{222}Rn/^{220}Rn	1.34	50%	88%	63%
D	P ~ FCO_2	-	-	-	-

4. DISCUSSION

The mapped soil gas concentrations and fluxes interpolated using sGs are shown in the succeeding figures. For each map, the anomaly threshold (AT) is represented as a contour line bounding the high values. Color scale ranges have been standardized for each soil gas across different areas to aid comparisons.

4.1 Soil gas anomalies in Area A

Overall, the gas anomalies in Area A fit spatially well together (Figure 4). In this sector, the highest radon (AT=11,467 Bq/m^3) and thoron concentrations (AT=8,510 Bq/m^3) were measured in the northern portion of the area, particularly at points along the Mahanagdong Flank Crater and its intersection with the North Mamban and Mantugop faults (No. 1 and 2 in Figure 4, respectively), which is consistent with the results of the 2013 radon survey. The north-south trending North Mamban Fault was intersected by production wells targeted to the east. Both well A-36 and A-27 indicated good permeability characteristics, *i.e.* shearing/veining, mud circulation losses, and faster rates of penetration in its intersection at this fault (Esperidion and Bien, 2004; Vicedo, 1996), while wells A-5, A-18, and A-34 reported tight or poor permeability in their intersection with this structure (Tebar, 1983; Alincastre, 1994; Palma and Bien, 2003).

High radon/thoron ratios (AT=2.32), on the other hand, are only evident on the juncture of the northeast-southwest trending Mantugop faults with the Mahanagdong flank crater (No. 2, Figure 4). This can denote a deeper gas source emanation along this structural intercept. The thoron anomaly also extends southwest following the Mantugop-D fault, which appears to be the favored degassing zone in this area. CO_2 flux anomalies (AT=24.34 g·m^{-2}·d^{-1}) also appear along the Mantugop faults and manifest strongly

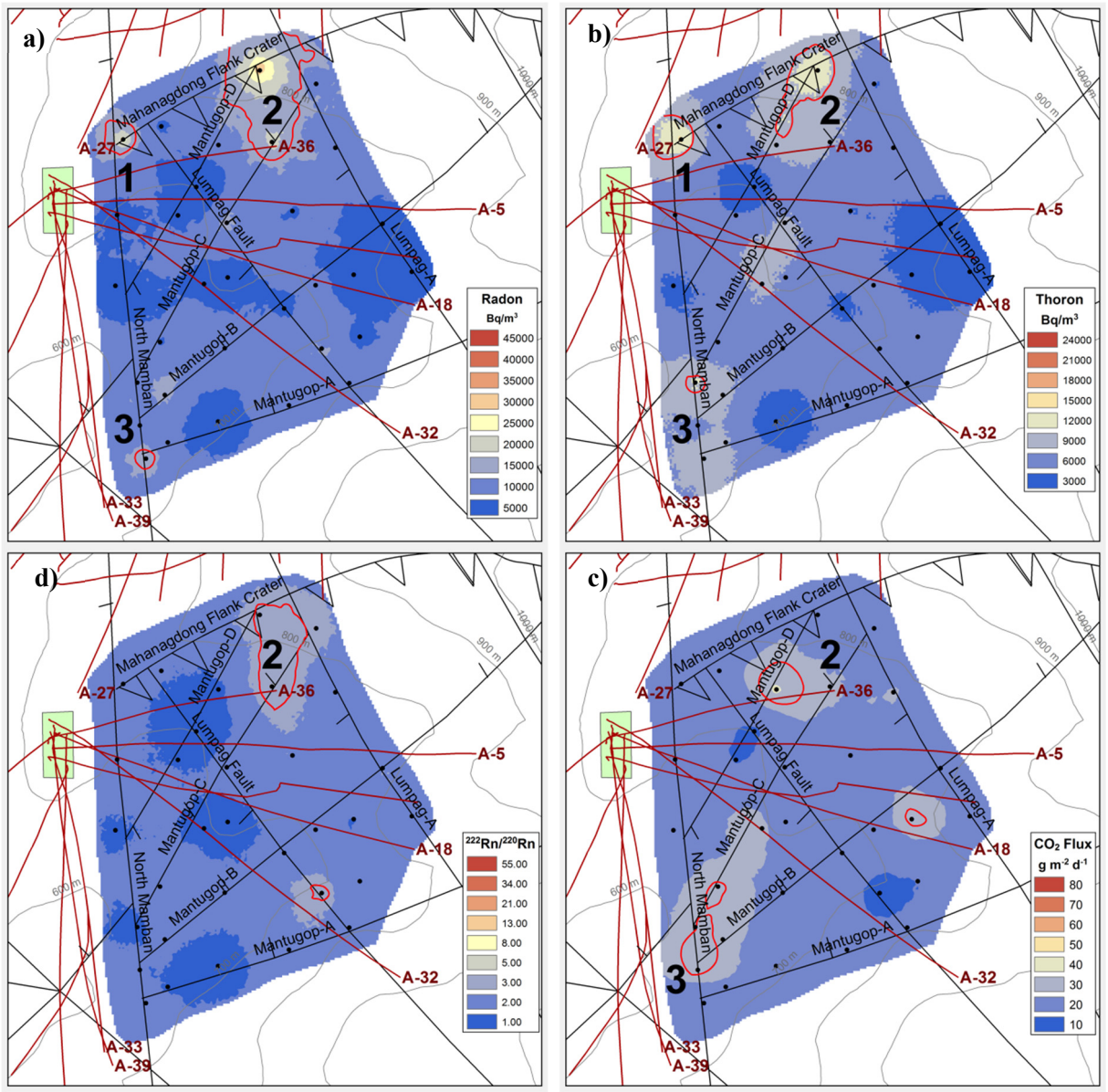

FIGURE 4: Soil gas anomaly maps in Area A. Clockwise from top left: radon (a), thoron (b), CO_2 flux (c), and radon/thoron ratio (d). Anomalies enclosed in red contours

in the closely-spaced intersections of the Mantugop faults with the North Mamban fault (No. 3 in Figure 4). Equivalently, wells A-33 and A-39 have good permeable zones attributable to this segment of the North Mamban fault (Herras, 1997; Bien and Contemplacion, 2007). The agreement of the anomalies in the production sector indicates that radon and thoron is carried mostly by CO_2 through these structures/structural segments.

4.2 Soil gas anomalies in Area B

Unlike Area A, in Area B the most discernible anomalies of each soil gas are absent in the other (Figure 5). For the related soil gases radon and thoron, the general trends are still similar despite variations in the highlighted anomaly.

A prominent radon anomaly (AT=23,300 Bq/m^3) can be seen bounded by the Central Fault Line, Cabalonan-A fault, and the parallel northeast trending Kinuhaan West and Kinuhaan-C Faults (No. 1 in Figure 5), with its highest reading at the Cabalonan-A fault. This is in agreement with good permeabilities encountered by wells B-7 (Leynes, 1996a) and B-8 (Bien, 1996) through Cabalonan-A

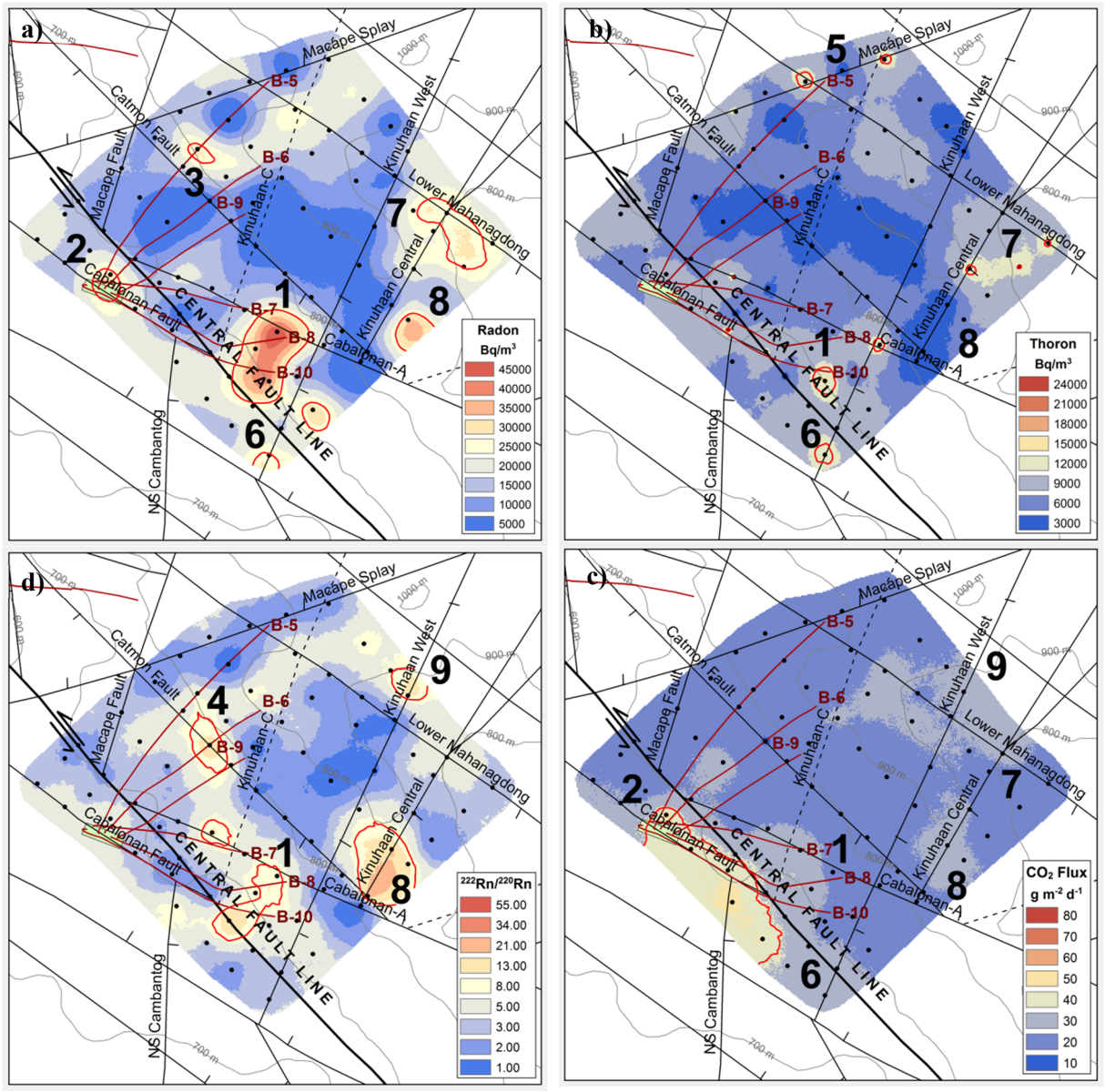

FIGURE 5: Soil gas anomaly maps in Area B. Clockwise from top left: radon (a), thoron (b), CO_2 flux (c), and radon/thoron ratio (d). Anomalies enclosed in red contours

fault. Kinuhaan-C fault is also described as one of the markedly permeable structures intersected by well B-10 (Bien and Palma, 2005).The existence of thoron activity (AT=9,923 Bq/m^3) and radon/thoron ratio(AT=6.19) anomalies also affirm that this area is a major degassing zone.

A contiguous CO_2 flux anomaly (AT=32.1 g·m^{-2}·d^{-1}) exists west of the Central Fault Line (No.2 in Figure 5). This anomaly follows the trace of the Cabalonan fault. A small radon anomaly is also present along this structure and around the well pad. This is consistent with the results of 2013 radon survey. Well B-10, whose track is parallel to the Cabalonan fault, had some indications of permeability at this structure, *i.e.*, intense argillization, influx of hematite and goethite, drusy veins and shearing, and circulation losses (Bien and Palma, 2005). The Central Fault Line, a splay of the Philippine Fault, is a regional structure running the whole length of the geothermal field. It is believed that this structure sets the western boundary of the shear zone, and consequently of permeability, in Leyte geothermal field (Caranto and Jara, 2015). Most of the wells drilled west of this structure reported poor permeability. In particular, all wells in Area B encountered weak shearing and minimal circulation losses through this structure. Even so, measurements along this structure are not distinctively low.

Wells B-5, B-6 and B-9 attribute their most productive zones to the east-northeast trending Catmon fault (Vicedo and Medrano Jr., 1995; Vicedo, 1997; Leynes, 1996b), and this was seen as high radon anomalies in 2013.However, distinct anomalies were not encountered, except for one or two high radon and thoron readings. A radon anomaly close to Catmon fault (No. 3, Figure 5) may be a manifestation of degassing. The anomaly along Catmon fault seen at the ratio map (No. 4, Figure 5) is caused by low radon and very low thoron values. It is therefore important to scrutinize anomaly distributions further because radon/thoron ratio anomalies can yield erroneous deductions, unless corroborated by radon or thoron. Well B-5 also has a permeable zone attributable to the overlap of Macape Splay and Lower Mahanagdong fault (Vicedo and Medrano Jr., 1995), which is also affirmed by a thoron anomaly (No. 5, Figure 5) in the same fault intersection.

Anomalies located along faults and fault intersections are also distributed throughout Area B (Nos. 6, 7, 8, 9 in Figure 5). No. 6 located in Kinuhaan West has consistent radon and thoron anomalies, and elevated CO_2 flux. No. 7 is a large radon anomaly in the intersection of Lower Mahanagdong and Kinuhaan West faults, with minor thoron anomalies and elevated CO_2 fluxes along the Lower Mahanagdong fault. These anomalies are indicative of degassing zones and good vertical permeability.

A radon anomaly south of Kinuhaan Central (No. 8, Figure 5) also has an elevated CO_2 flux. Despite the presence of ratio anomalies and elevated CO_2 flux along the western terminus of Kinuhaan fault, the radon concentrations are very low, and thus minimal vertical permeability is presumed for the structure. Same deduction can be made for a ratio anomaly and elevated CO_2 flux at the eastern segment of Kinuhaan West (No. 9, Figure 5), without accompanying high radon readings.

4.3 Soil gas anomalies in Area C

In Area C, it is important to look at the relationships and concurrence of anomalies to discern the degassing structures. Radon and thoron patterns (and their ratio) can suggest dynamics with regards to the depths of origin of these gases. However, the connotation of a deep or shallow source is not of a quantified depth, but rather referring only to the relative vertical distances that can be traveled by radon and thoron considering their short half-lives. For the radon (AT=25,367 Bq/m^3), thoron (AT=13,000 Bq/m3), and radon/thoron ratio maps (AT=4.17), there are four principal patterns. First is the observed persistent anomaly of both radon and thoron, occurring along the north-northeast trending Concepcion fault (No. 1, Figure 6), the northern terminus of the north-northwest-trending Cabalonan-B fault (No. 2, Figure 6), a probable extension of Catmon fault (No. 3, Figure 6), and a fault west of the Central Fault Line with an apparent extension east of the Central Fault Line (No. 4, Figure 6).The presence of a very high radon concentration, coupled with a high thoron concentration indicates very good conduction of deep gases through continuously permeable vertical channels. A CO_2 flux anomaly (AT=40.78 $g \cdot m^{-2} \cdot d^{-1}$) has been observed along No. 1, while elevated flux values correspond to Nos. 2, 3, and 4.

The second case is the occurrence of radon anomalies accompanied by radon/thoron ratio anomalies, such as No. 5, located on Lower Mahanagdong and its intercepts with NE-Janagdan, Pangog, and EW Cabalonan faults, and No. 6, west of Central Fault Line, at Imelda North Fault. The anomaly at No. 5 is supported by a sizeable area of elevated CO_2 flux, while at No. 6 there is a high CO_2 flux trend following the Central Fault Line. These radon anomalies have also been encountered in the previous radon survey. The presence of high radon in all these structures may indicate good permeability from deep sources, but slower transport in soil or at the shallower depths resulted in lower thoron values being measured, and thus higher ratios being observed.

The third observation is the occurrence of thoron anomalies only, found at the EW Cabalonan fault (No. 7, Figure 6) and the Cabalonan-A fault (No. 8, Figure 6). In almost all cases, anomalous thoron is accompanied by a fairly high radon concentration. CO_2 flux anomalies do not coincide with thoron anomalies but high concentrations are located in these spots. The abundance of thoron can be explained by the presence of structures with good permeability but restricted at shallower depths.

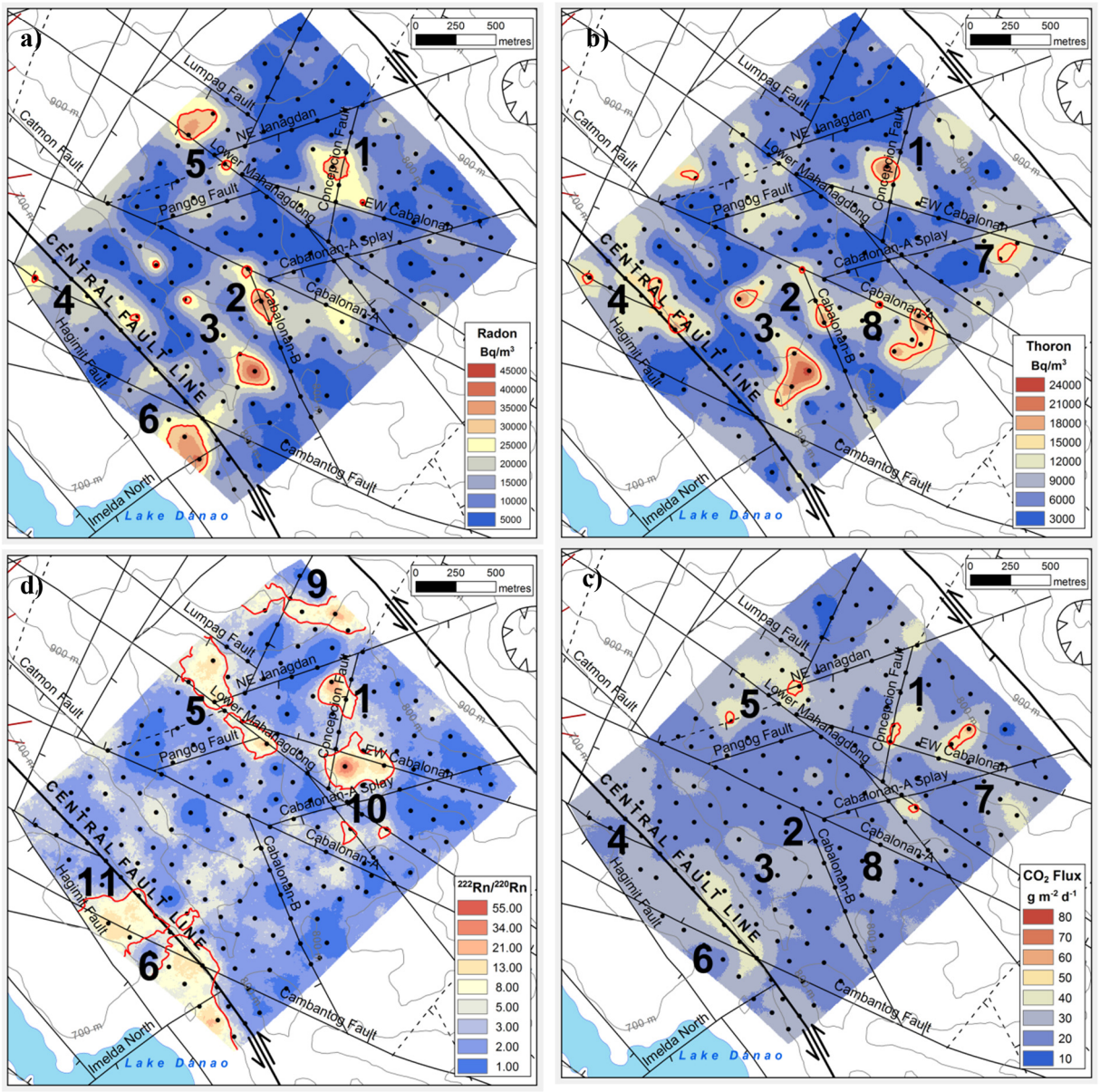

FIGURE 6: Soil gas anomaly maps in Area C. Clockwise from top left: radon (a), thoron (b), CO_2 flux (c), and radon/thoron ratio (d). Anomalies enclosed in red contours

The fourth case is the occurrence of only ratio anomalies. Such stations occur at the north-northeast trending NW Janagdan splay (No. 9, Figure 6), the west-southwest trending EW Cabalonan fault (No. 10, Figure 6), and the area east of the Central Fault Line along Cambantog fault (No. 11, Figure 6). Closer inspection shows that these anomalous ratios are reflections of low values for radon and much lower ratios for thoron. Since no radon or thoron anomalies are present, these “false anomalies” may not signify the presence of good vertical permeability. This kind of anomaly may also denote very poor soil permeability. For example, the area east of the Central Fault is a stream valley and several spots are swampy year-round. In this area have low radon values and almost zero thoron values were measured, likely due to water saturation of underlying strata.

5. CONCLUSIONS

The soil gas survey conducted in Mahanagdong geothermal field showed that soil gas anomalies can be correlated to the permeability characteristics of structures. It is possible to model the relationship between soil gases and permeability using logistic regression and obtain a permeability threshold, although this resulted in broad general anomalies. Certainly, improvements can be done with the sample size by the addition of measurements from well-fault intersections to further evaluate the models. Nonetheless, delineating structural zones of interest can be done with a partitioning method. This resulted in compact anomalies that in most cases can be associated with a structural feature.

Very high values of radon, thoron and CO_2 flux has been measured in soil close to thermal areas, confirming that convecting geothermal fluids are enriched in these gases. However, small and localized environments may exist at near surface that can exert control on the diffuse emanation of trace gases, which can lead to low measurements as well.

Radon, thoron, and radon/thoron ratio can be useful in the inference of the gas source depth. Concurrence of radon and thoron anomalies suggests very good conduction of gases from deep sources through continuously permeable vertical conduits. A high radon and radon/thoron ratio can indicate good permeability and advection from deep sources, while a high thoron will indicate a shallow gas source and good permeability only at shallow depths.

The CO_2 flux anomalies are not in strong agreement with the anomalies of the radioactive gases, but elevated CO_2 fluxes are still observed in most instances. Nevertheless, the occurrence of high fluxes with high radon and thoron measurements will indicate that CO_2 functions as the major carrier gas of radon and thoron. In several cases it has also been demonstrated that gases may follow a favorable degassing zone. In turn, this offers an alternative assumption for the logistic regression model that vertical permeability may not always be continuous.

ACKNOWLEDGEMENTS

I am extremely indebted to the United Nations University – Geothermal Training Programme, for providing us the opportunity to learn from geothermal experts and further our knowledge in this field. My deepest gratitude goes out to the people who foster this institution, the director, Lúdvík S. Georgsson, deputy director, Ingimar G. Haraldsson, and staff, Thórhildur Ísberg, María S. Gudjónsdóttir, Málfrídur Ómarsdóttir, and Markús A.G. Wilde, for all their help in almost every aspect of living here in Iceland and for ensuring that we maximize our experience and learning. I would also like to express my appreciation to the staff of ÍSOR, Orkustofnun, and our lecturers for sharing their knowledge and expertise with us fellows, especially to Finnbogi Óskarsson for his guidance during our specialized training. I am very thankful for my advisor, Audur Agla Óladóttir for giving good counsel along the course of the project work and for imparting helpful thoughts and ideas that shaped this report. My participation in this programme would not have been possible if not for the grace and vision of Energy Development Corporation (EDC), through Mr. Manuel S.Ogena, Ka Noel D. Salonga, Mr. Francis M. Sta. Ana, Mr. Joeffrey A. Caranto, and Ms. Rosella G. Dulce. Thank you for this opportunity. A million thanks also to Atoz A.Vasquez, who has been the other half of this study, for his valuable reviews, and for his dedication to this project. I would also like to thank my colleagues at EDC, whom I find pleasure working with, for job-related assistance and much needed encouragements. I am very grateful to the 2015 UNU Fellows for sharing this awesome learning and life experience with them. In the future, I hope to meet these amazing people as experts in their respective fields. And to all the friends I've made here in Iceland, thank you for the kindness and friendship. Trust that we will meet again in the future. To my housemates at Fýlshólar, Lee, Jason, and Bryan, I can never be grateful enough for the friendship and all the good times. Lastly, I wish to thank my loving mom, my brother and sisters, relatives and friends back home, who have been very supportive and proud of my endeavours. This is dedicated to all of you.

REFERENCES

Alincastre, R.S., 1994: *Geology of well MG-18D.*Philippine National Oil Company – Energy Development Company, Taguig City, Philippines, internal report, 28 pp.

Allard, P., Carbonnelle, J., Dajlevic, D., Le Bronec, J., Morel, P., Robe, M.C., Maurenas, J.M., Faivre-Pierret, R., Martin, D., and Sabroux, J.C.,1991: Eruptive and diffuse emissions of CO_2 from Mount Etna. *Nature*, *351*, 387–391.

Bergfeld, D., Goff, F., and Janik, C.J., 2001: Elevated carbon dioxide flux at the Dixie Valley geothermal field, Nevada; relations between surface phenomena and the geothermal reservoir. *Chemical Geology*, *177*, 43–66.

Bien, O.C., 1996: *Geology of MG-8RD*. Philippine National Oil Company – Energy Development Company, Taguig City, Philippines, internal report, 52 pp.

Bien, O.C., and Contemplacion, R.D., 2007: *Geology of well MG39D.*Philippine National Oil Company – Energy Development Company, Taguig City, Philippines, internal report, 30 pp.

Bien, O.C., and Palma, R.R., 2005: *Geologic report of well MG-10RD.*Philippine National Oil Company – Energy Development Company, Taguig City, Philippines, internal report, 27 pp.

Brusca, L., Inguaggiato, S., Longo, M., Madonia, P., and Maugeri, R., 2004: The 2002-2003 eruption of Stromboli (Italy): Evaluation of the volcanic activity by means of continuous monitoring of soil temperature, CO_2 flux and meteorological parameters. *Geochemistry, Geophysics, Geosystems*, *5*, 14 pp.

Caranto, J.A., and Jara, M.P., 2015: Factors controlling reservoir permeability at the Leyte geothermal field, Philippines.*Proceedings of the World Geothermal Congress 2015, Melbourne, Australia,* 8 pp.

Chiodini, G., Cioni, R., Guidi, M., Raco, B., and Marini, L., 1998: Soil CO_2 flux measurements in volcanic and geothermal areas. *Applied Geochemistry*, *13*, 543–552.

Cox, M.E., 1980: Ground radon survey of a geothermal area in Hawaii. *Geophysical Research Letters*, *7*, 283–286.

Delfin, F.G., and Tebar, H.J., 1986: Geologic structures at the Mahiao, Sambaloran and Malitbog sectors of the Tongonan geothermal field, Leyte, Philippines.*Proceedings of the 8th New Zealand Geothermal Workshop*, 129–134.

Delmelle, P., and Stix, J., 1999: Volcanic gases. In Sigurdsson, H.,Houghton, B.,Rymer, H.,Stix, J., and McNutt, S. (eds.), *Encyclopedia of Volcanoes.*Academic Press, 803–816.

Deutsch, C.V., and Journel, A.G., 1998: *GSLIB: Geostatistical software library and user's guide*. Oxford University Press, New York, NY, United States, 384 pp.

Esperidion, J.A., and Bien, O.C., 2004: *Well MG-36D geology report.*Philippine National Oil Company – Energy Development Company, Taguig City, Philippines, internal report, 30 pp.

Fleischer, R.L., and Mogro-Campero, A., 1978: Mapping of integrated radon emanation for detection of long-distance migration of gases within the Earth: Techniques and principles. *Journal of Geophysical Research: Solid Earth*, *83*, 3539–3549.

Fridriksson, Th., Kristjánsson, B.R., Ármannsson, H., Margrétardóttir, E., Ólafsdóttir, S., and Chiodini, G., 2006: CO_2 emissions and heat flow through soil, fumaroles, and steam heated mud pools at the Reykjanes geothermal area, SW Iceland. *Applied Geochemistry*, *21*, 1551–1569.

Frondini, F., Chiodini, G., Caliro, S., Cardellini, C., Granieri, D., and Ventura, G., 2004: Diffuse CO_2 degassing at Vesuvio, Italy. *Bulletin of Volcanology*, *66*, 642–651.

Giammanco, S., Immè, G., Mangano, G., Morelli, D., and Neri, M., 2009: Comparison between different methodologies for detecting radon in soil along an active fault: The case of the Pernicana fault system, Mt. Etna (Italy). *Applied Radiation and Isotopes*, *67*, 178–185.

Heiligmann, M., Stix, J., Williams-Jones, G., Lollar, B.S., and Gustavo Garzón, V., 1997: Distal degassing of radon and carbon dioxide on Galeras volcano, Colombia. *Journal of Volcanology and Geothermal Research*, *77*, 267–283.

Herras, E.B., 1997: *Geology of well MG-33D.*Philippine National Oil Company – Energy Development Company, Taguig City, Philippines, internal report, 24 pp.

Hinkle, M.E., 1991: Seasonal and geothermal production variations in concentrations of He and CO_2 in soil gases, Roosevelt Hot Springs known geothermal resource area, Utah, U.S.A. *Applied Geochemistry*, *6*, 35–47.

Jolie, E., Klinkmueller, M., and Moeck, I., 2015: Diffuse degassing measurements in geothermal exploration of fault controlled systems. *Proceedings of the World Geothermal Congress 2015, Melbourne, Australia*, 8 pp.

Klusman, R.W., Moore, J.N., and LeRoy, M.P., 2000: Potential for surface gas flux measurements in exploration and surface evaluation of geothermal resources. *Geothermics*, *29*, 637–670.

Lewicki, J.L., and Oldenburg, C.M., 2004: *Strategies for detecting hidden geothermal systems by near-surface gas monitoring.* Lawrence Berkeley National Laboratory, Berkeley, CA, United States,report no. LBNL-56895, 76 pp.

Leynes, R.D., 1996a: *Geology of well MG-7RD.*Philippine National Oil Company – Energy Development Company, Taguig City, Philippines, internal report, 35 pp.

Leynes, R.D., 1996b: *Geology of Well MG-6RD*. Philippine National Oil Company – Energy Development Company, Taguig City, Philippines, internal report, 42 pp.

Mahon, W.A.J., McDowell, G.D., and Finlayson, J.B., 1980: Carbon dioxide: its role in geothermal systems. *New Zealand Journal of Science*, *23*, 133–148.

McCarthy, J.H., and Reimer, G.M., 1986: Advances in soil gas geochemical exploration for natural resources: Some current examples and practices. *Journal of Geophysical Research: Solid Earth*, *91*, 12327–12338.

Mismanos, J., and Vasquez, A., 2013: *Soil radon gas survey in Mahanagdong, Leyte: integrated final report.* Energy Development Corporation, Pasig City, Philippines,internal report, 64 pp.

Óladóttir, A.A., and Fridriksson, Th., 2015: The evolution of CO_2emissions and heat flow through soil since 2004 in the utilized Reykjanes geothermal area, SW Iceland: Ten years of observations on changes in geothermal surface activity. *Proceedings of the World Geothermal Congress 2015, Melbourne, Australia*, 10 pp.

Padrón, E., López, D.L., Magaña, M.I., Marrero, R., and Pérez, N.M., 2003: Diffuse degassing and relation to structural flow paths at Ahuachapán geothermal field, El Salvador. *Geothermal Resources Council Transactions*, *27,* 325–330.

Palma, R.R., and Bien, O.C., 2003: *Geology report of well MG-34D.*Philippine National Oil Company – Energy Development Company, Taguig City, Philippines, internal report, 23 pp.

Parker, R.L., 1967: Composition of the earth's crust. In: Fleischer, M. (ed.), *Data of geochemistry* (6th ed.). United States Government Printing Office, Washington D.C., United States, D1-D19.

Rinaldi, A.P., Vandemeulebrouck, J., Todesco, M., and Viveiros, F., 2012: Effects of atmospheric conditions on surface diffuse degassing. *Journal of Geophysical Research*, *117*, 14 pp.

Rochette, P., and Hutchinson, G.L., 2005: *Measurement of soil respiration in situ: chamber techniques.* University of Nebraska, Lincoln, NE, United States, 40 pp.

Rodríguez, A., Torres, Y., Chavarría, L., and Molina, F., 2008: Soil gas radon measurements as a tool to identify permeable zones at Las Pailasgeothermal area, Costa Rica. *Presented at the "30th Anniversary Workshop", organized by UNU-GTP, in Reykjavik, Iceland*, 7 pp.

Seastres Jr., J.S., Salonga, N.D., and Saw, V.S., 1996: Hydrology of the greater Tongonangeothermal system, Philippines and its implications to field exploitation. *Geothermal Resources Council Transactions*, *20,* 713–720.

Semprini, L., and Kruger, P., 1983: Simulation of radon transport in geothermal reservoirs. *Proceedings of the 9th Workshop on Geothermal Reservoir Engineering,*Stanford University, Stanford, CA, United States, 261-268.

Sinclair, A.J., 1974: Selection of threshold values in geochemical data using probability graphs. *Journal of Geochemical Exploration*, *3*, 129–149.

Sinclair, A.J., 1991: A fundamental approach to threshold estimation in exploration geochemistry: probability plots revisited. *Journal of Geochemical Exploration*, *41*, 1–22.

Tanner, A.B., 1980: Radon migration in the ground: a supplementary review. *Natural Radiation Environment III*, *1*, 5–56.

Tebar, H.J., 1983: *Well MG-5D preliminary geologic report.*Philippine National Oil Company – Energy Development Company, Taguig City, Philippines, internal report, 10 pp.

Vicedo, R.O., 1996: *Geology of well MG-27D.*Philippine National Oil Company – Energy Development Company, Taguig City, Philippines, internal report, 25 pp.

Vicedo, R.O., 1997: *Geology of well MG-9RD.*Philippine National Oil Company – Energy Development Company, Taguig City, Philippines, internal report, 21 pp.

Vicedo, R.O., and Medrano Jr., R.A., 1995: *Geology of well MG-5RD.*Philippine National Oil Company – Energy Development Company, Taguig City, Philippines, internal report, 39 pp.

Voltattorni, N., and Lombardi, S., 2010: Soil gas geochemistry: significance and application in geological prospectings. In: Potocnik, P. (ed.), *Natural Gas*. Sciyo, 183-204.

Voltattorni, N., Sciarra, A., and Quattrocchi, F., 2010: The application of soil gas technique to geothermal exploration: study of "hidden" potential geothermal systems. *Proceedings of the World Geothermal Congress 2010, Bali, Indonesia*, 7 pp.

Ward, C.W., 1979: The geology and hydrothermal alteration of the Tongonan geothermal field. *Proceedings of the New Zealand Geothermal Workshop,* 113–125.

Werner, C., and Cardellini, C., 2006: Comparison of carbon dioxide emissions with fluid upflow, chemistry, and geologic structures at the Rotorua geothermal system, New Zealand. *Geothermics*, *35*, 221–238.

Witcher, J.C., 1991: Radon soil-gas surveys with diffusion-model corrections in geothermal exploration. *Geothermal Resources Council Transactions*, *15*, 301–308.

Yang, T.F., Walia, V., Chyi, L.L., Fu, C.C., Chen, C.H., Liu, T.K., Song, S.R., Lee, C.Y., and Lee, M., 2005: Variations of soil radon and thoron concentrations in a fault zone and prospective earthquakes in SW Taiwan. *Radiation Measurements*, *40*, 496–502.

APPENDIX I: Probability plots of data sets from Areas A, B, and C

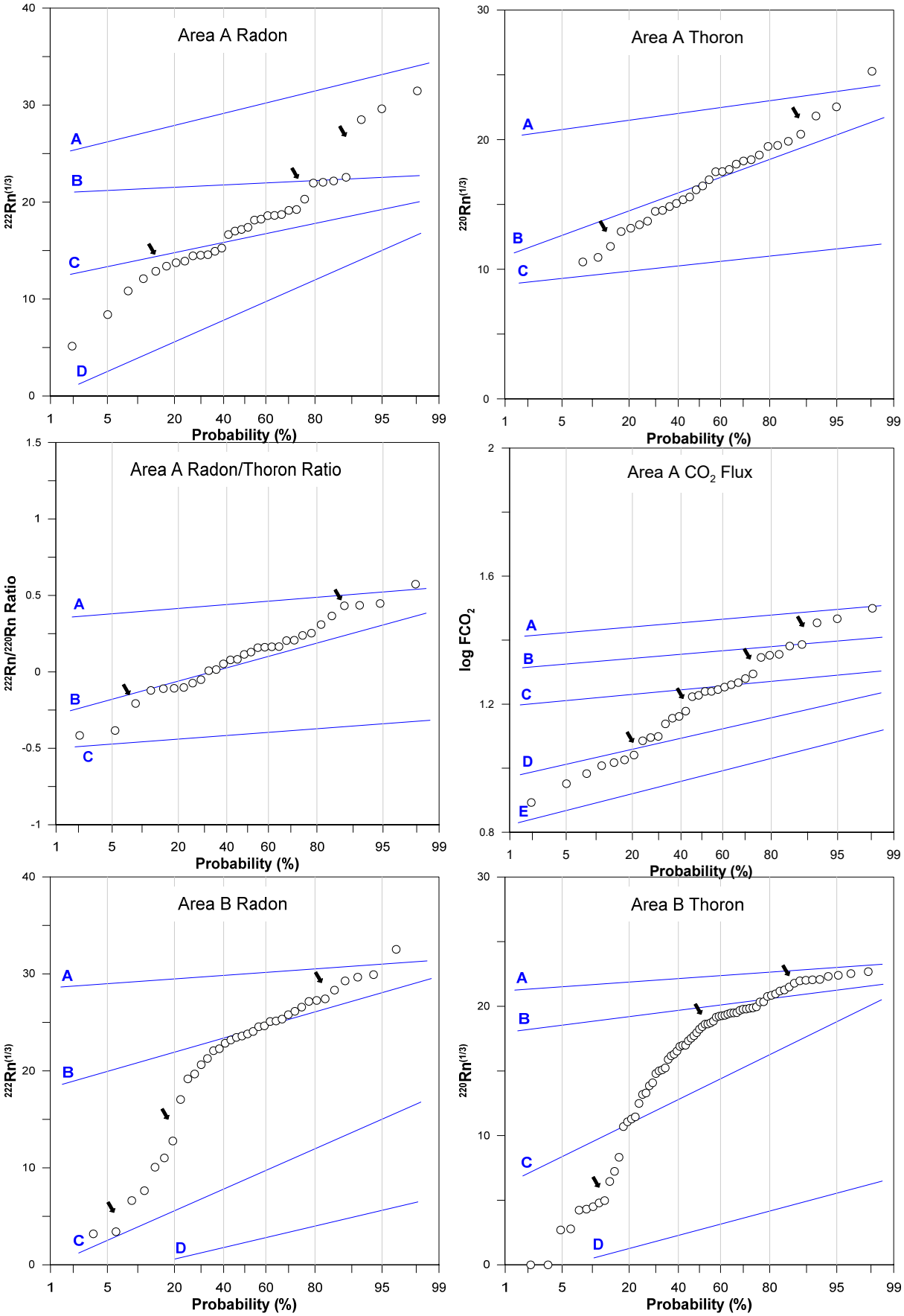

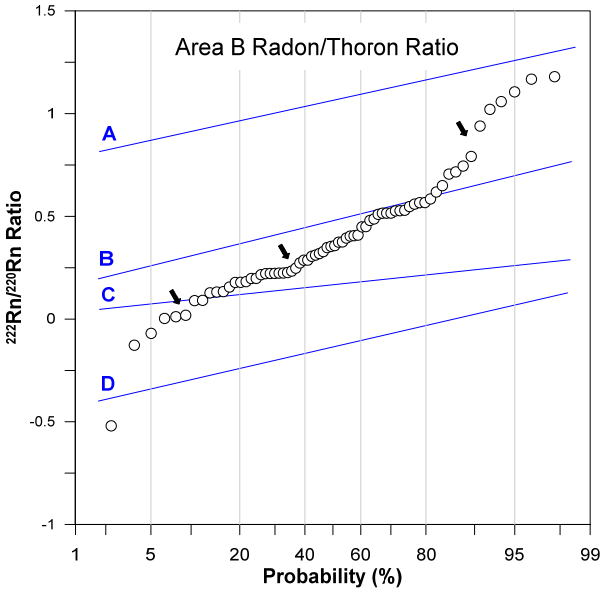
Area B Radon/Thoron Ratio
222Rn/220Rn Ratio
Probability (%)
A
B
C
D

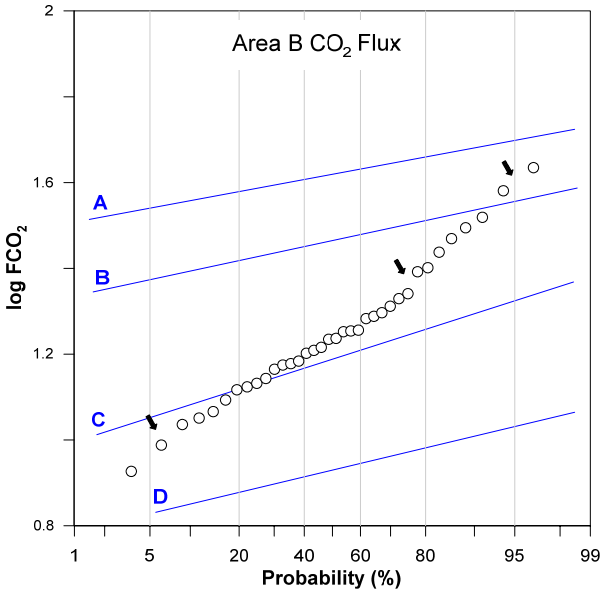
Area B CO2 Flux
log FCO2
Probability (%)
A
B
C
D

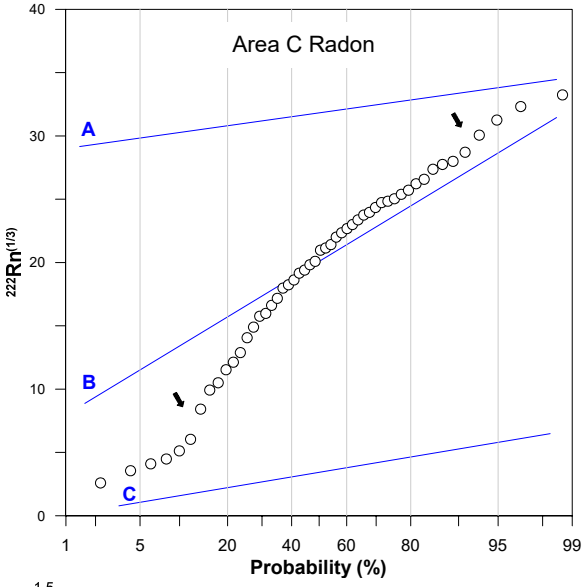
Area C Radon
222Rn(1/3)
Probability (%)
A
B
C

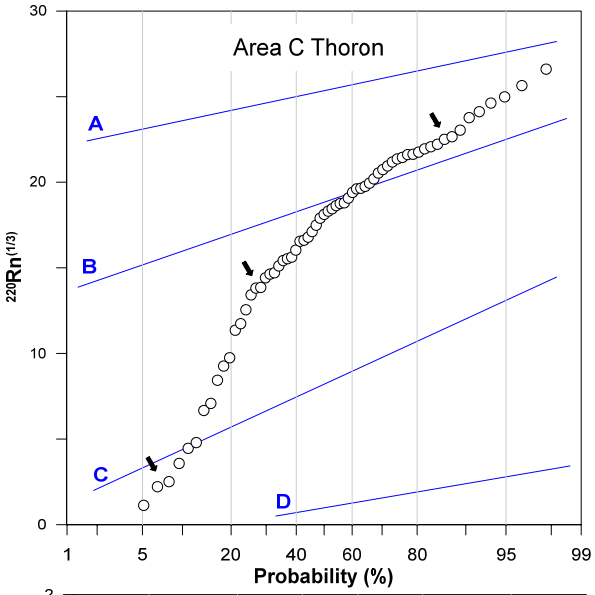
Area C Thoron
220Rn(1/3)
Probability (%)
A
B
C
D

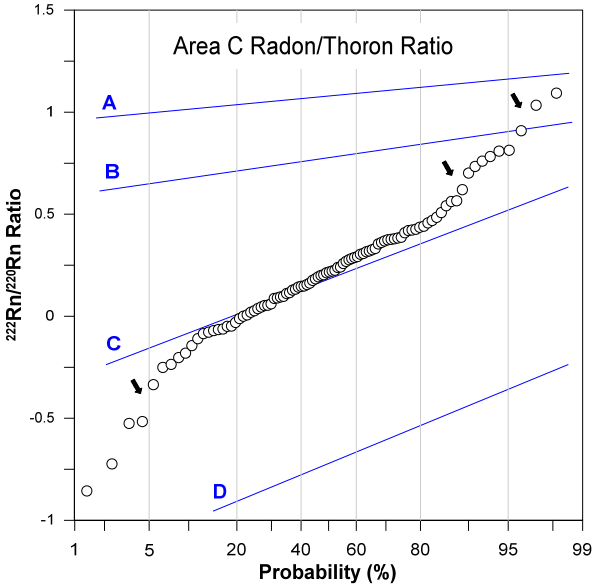
Area C Radon/Thoron Ratio
222Rn/220Rn Ratio
Probability (%)
A
B
C
D

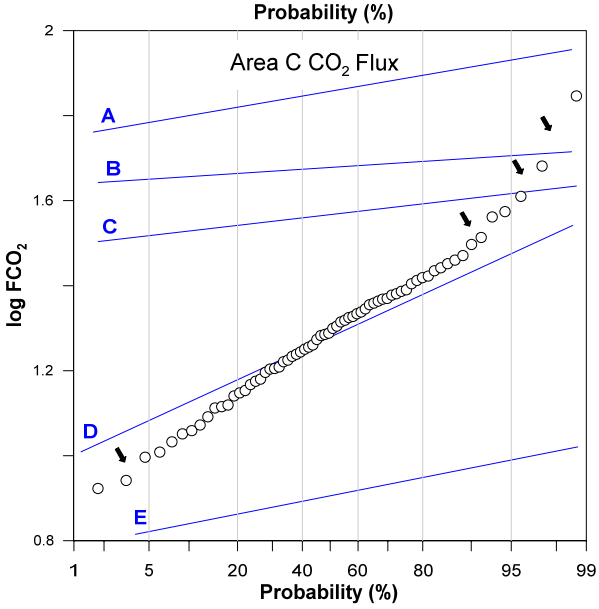
Area C CO2 Flux
log FCO2
Probability (%)
A
B
C
D
E

APPENDIX II: Results of the partitioning of populations

	Area A		Area B		Area C		Characteristic
	N	range	*N*	range	*N*	range	
Radon Bq/m^3	3	11467–31100	9	23300–45300	15	25367–45900	Anomaly
	4	8367–11467	49	4957–23333	167	220–25367	Background
	21	1770–8363	13	30–4957	25	0–220	Background
	4	136–1770	4	0–33			Background
Thoron Bq/m^3	3	8510–11600	10	9923–14900	21	13000–23400	Anomaly
	24	1627–8510	27	6057–9923	132	2457–13000	Background
	5	0–1627	29	110–6057	37	16–2457	Background
			9	0–110	17	0–16	Background
Radon/ Thoron					6	8.22-61.03	Anomaly
	4	2.32-3.74	7	6.19-20.77	15	4.17-8.22	Anomaly
	24	0.41-2.32	40	1.68-6.19	165	0.31-4.17	Background
	2	0.38-0.41	18	1.04-1.68	10	0.08-0.31	Background
			7	0.27-1.04			Background
CO_2 Flux g·m^{-2}·d^{-1}					4	50.57–79.04	Anomaly
	3	24.34–31.58	4	32.1–82.69	3	40.78–50.57	Anomaly
	5	19.70–24.34	13	22.64–32.1	10	32.61–40.78	Background
	10	15.07–19.70	53	9.73–22.64	181	9.72–32.61	Background
	8	10.62–15.07	5	4.98–9.73	9	4.90–9.72	Background
	6	7.81–10.62					Background